Journal of Biomolecular NMR (2006) 34: 89–100
DOI 10.1007/s10858-005-5583-6

Article

Structural basis for non-covalent interaction between ubiquitin and the ubiquitin conjugating enzyme variant human MMS2

Michael J. Lewis[a], Linda F. Saltibus[a], D. Duong Hau[a], Wei Xiao[b] & Leo Spyracopoulos[a,*]

[a]*Department of Biochemistry, University of Alberta, Edmonton, Alberta, T6G 2H7, Canada;* [b]*Department of Microbiology and Immunology, University of Saskatchewan, Saskatoon, Saskatchewan, S7N 5E5, Canada*

Received 31 May 2005; Accepted 9 November 2005

Key words: K63, mms2, polyubiquitination, ubiquitin, ubiquitin binding motif, UEV

Abstract

Modification of proteins by post-translational covalent attachment of a single, or chain, of ubiquitin molecules serves as a signaling mechanism for a number of regulatory functions in eukaryotic cells. For example, proteins tagged with lysine-63 linked polyubiquitin chains are involved in error-free DNA repair. The catalysis of lysine-63 linked polyubiquitin chains involves the sequential activity of three enzymes (E1, E2, and E3) that ultimately transfer a ubiquitin thiolester intermediate to a protein target. The E2 responsible for catalysis of lysine-63 linked polyubiquitination is a protein heterodimer consisting of a canonical E2 known as Ubc13, and an E2-like protein, or ubiquitin conjugating enzyme variant (UEV), known as Mms2. We have determined the solution structure of the complex formed by human Mms2 and ubiquitin using high resolution, solution state nuclear magnetic resonance (NMR) spectroscopy. The structure of the Mms2–Ub complex provides important insights into the molecular basis underlying the catalysis of lysine-63 linked polyubiquitin chains.

Abbreviations: Ub – ubiquitin; E1 – ubiquitin activating enzyme; E2 – ubiquitin conjugating enzyme; E3 – ubiquitin ligase; UEV – ubiquitin conjugating enzyme variant; CUE – similar to yeast protein Cue1p; UBA – ubiquitin associated domain; UIM – ubiquitin interacting motif; NMR – nuclear magnetic resonance; ITC – isothermal titration calorimetry; IPTG – isopropyl ß-D-thiogalactopyranoside; NOE – nuclear Overhauser effect.

The post-translational addition of ubiquitin Ub[1] to a target protein plays a pivotal role in the regulation of cell processes in eukaryotes (Chan and Hill, 2001; Ben-Neriah, 2002; Glickman and Ciechanover, 2002). In the most studied pathway, polyubiquitin chains linked through Lys48 serve to target proteins for degradation by the 26S proteasome (Glickman and Ciechanover, 2002). The first step of this process involves the covalent attachment of the C-terminus of Ub (Gly76) to the active site cysteine of a ubiquitin activating enzyme (E1), where it is subsequently transferred as a thiolester intermediate to a ubiquitin conjugating enzyme (E2). Finally, Ub is attached to a target protein through the activity of a ubiquitin ligase (E3). Ultimately, polyubiquitin chains are built up by the formation of isopeptide bonds between Lys48 of one Ub and the C-terminus of a sequential Ub, through a mechanism for which the details are presently unknown.

Ubiquitin is involved in regulatory mechanisms in eukaryotes that are distinct from signaling for proteolysis. For example, protein

*To whom correspondence should be addressed. E-mail: leo.spyracopoulos@ualberta.ca

mono-ubiquitination is involved in vesicle budding, transcriptional regulation, and receptor endocytosis (Hicke, 2001; Haglund et al., 2003). Polyubiquitin chains linked through Lys63 have been implicated in error-free DNA repair (Broomfield et al., 1998; Hofmann and Pickart, 1999; Hoege et al., 2002), and NF-κB activation (Deng et al., 2000; Wang et al., 2001).

Lys63-linked polyubiquitin chains are covalently assembled by a protein heterodimer consisting of an E2 and a ubiquitin E2 variant, or UEV. UEVs are structurally similar to E2s, but lack the canonical active site cysteine residue that is necessary to catalyze isopeptide bond formation with the C-terminus of Ub. UEV domains comprise one type of structurally distinct ubiquitin binding motifs. Other ubiquitin binding motifs include CUE (similar to yeast Cue1p), UBA (Ub associated domain), and UIM (Ub interacting motif) (Schnell and Hicke, 2003). The ubiquitin binding properties of these motifs are variable, and have been recently reviewed (Hicke et al., 2005).

In yeast, Lys63-linked polyubiquitin chains function in the post-transcriptional DNA repair pathway (Broomfield et al., 1998; Hofmann and Pickart, 1999). The chains are assembled by a heterodimer consisting of Ubc13, a typical E2, and Mms2, a UEV. The human homologue of the Mms2–Ubc13 complex has been identified, and shown to complement DNA repair defects in yeast, implicating this complex for DNA repair in humans (Xiao et al., 1998).

A mechanism for Lys63-linked chain catalysis has been proposed based on a combination of X-ray crystallography (Moraes et al., 2001), NMR (McKenna et al., 2001; McKenna et al., 2003b; McKenna et al., 2003a), and ITC (McKenna et al., 2003a) studies. For this model, the active site cysteine of hUbc13 is covalently attached to the C-terminus of a "donor" Ub, and hMms2 is non-covalently associated with an "acceptor" Ub whose Lys63 is proximal to the active site cysteine of hUbc13. Of the three major protein–protein interactions in the tetramer (E2–UEV, UEV–Ub, and E2–Ub), only the hMms2–hUbc13 complex has been characterized at high resolution using X-ray crystallography (Moraes et al., 2001). Crystallization of hMms2–hUbc13 with acceptor and/or donor Ub is difficult, presumably due to the low binding affinity between hMms2 and the acceptor Ub $K_D = 98 \pm 15$ (μM) (McKenna et al., 2003a), and the instability of the thiolester bond between hUbc13 and the donor Ub (Miura et al., 1999). In the present study, we have characterized the interaction between hMms2 and Ub, using high-resolution, solution-state NMR spectroscopy.

Materials and methods

Protein expression and purification

In order to determine the structure of the hMms2–Ub complex using solution state NMR spectroscopy, four NMR samples containing various proteins or combinations of proteins were prepared: ~2.0 mM [$U-^{15}$N; $U-^{13}$C]–Ubiquitin K48R and ~0.5 mM hMms2; ~0.5 mM [$U-^{15}$N; $U-^{13}$C]–hMms2 and ~2.0 mM Ubiquitin; ~0.7 mM [$U-^{15}$N; U-10% ^{13}C]-hMms2; and ~0.25 mM [$U-^{15}$N]–Ub titrated with successive aliquots of hMms2.

Ubiquitin

[$U-^{15}$N; $U-^{13}$C]–Ubiquitin K48R was expressed in *E. coli* strain BL21(DE3)-RIL in the following manner: 50 ml of LB medium (10 g/L bacto-tryptone, 5 g/L bacto-yeast extract and 10 g/L NaCl, pH 7.5) containing ~ 50 μg/mL ampicillin and ~25μg/mL chloramphenicol was inoculated with a single colony and allowed to grow to A_{600} ~ 0.9. About 2 mL of this culture was used to inoculate 2 L of M9 minimal media (Sambrook et al., 1989) containing 2 g/L [$^{13}C_6$, 99%] D-glucose as the sole carbon source and 1 g/L [^{15}N, 98%] ammonium sulfate as the sole nitrogen source. The media also contained 2 mM $MgSO_4$, 2 μM $FeSO_4$, 5 mg/L thiamine, 1 mL/L vitamin solution (Slupsky et al., 1995), 50 μg/mL ampicillin, and 25 μg/mL chloramphenicol.

The cells were grown at 25 °C with aeration to A_{600} ~ 0.8, and induced with 0.4 mM IPTG. The cells were grown for an additional 4 hours and harvested by centrifugation. The cell pellet was resuspended in lysis buffer (140 mM NaCl, 2.7 mM KCl, 10 mM Na_2HPO_4, 1.8 mM KH_2PO_4, 100 μg/mL DNase I, 1 mM DTT, 10 mM $MgSO_4$, 0.5% protease inhibitor cocktail II (Calbiochem catalog #538132)) and lysed by two passes through a French press. The lysate was clarified by centrifugation at 25,000 rpm in a

Beckman JA 25.5 rotor, and the supernatant was filtered through a Millipore steriflip 0.45 μm vacuum filtration device. The filtrate was loaded onto a HiLoad 26/10 Q-Sepharose column equilibrated with 50 mM TRIS, 1 mM EDTA, and 1 mM DTT, pH 7.0. Fractions eluting between 50 and 127 mL were pooled and passed over the Q-Sepharose column a second time. Fractions eluting between 50 and 200 mL were collected, concentrated to a volume of ~1.4 mL, and loaded onto a Hiload 26/60 Superdex 30 column. Fractions eluting at ~150 mL were collected and concentrated to ~2 mL using Amicon Ultra15 5 K and Millipore Ultrafree 0.5 BioMax 5 K centrifugal membrane filtration devices.

Ubiquitin K48R was expressed in *E. coli* strain BL21(DE3)-RIL. About 2 L cultures of LB media containing ~50 μg/mL ampicillin were grown at 37 °C to $A_{600} \sim 1.3$, subsequently induced with 0.4 mM IPTG, and allowed to grow ~12 hours. Bacterial cells were subjected to centrifugation at 5000 rpm in a Beckman JLA 10.5 rotor for 15 min and re-suspended in buffer containing 140 mM NaCl, 2.7 mM KCl, 10 mM Na_2HPO_4, 1.8 mM KH_2PO_4. Clarification of the cell lysate was achieved by centrifugation at 25000 rpm in a Beckman JA-25.5 rotor for 20 min followed by filtration through a Millipore steriflip 0.45 μm vacuum filtration unit. The filtered solution was passed two times through a Q-Sepharose HiLoad 26/10 ion-exchange column equilibrated in pH 7.0 buffer containing 50 mM TRIS, 1 mM DTT, and 1 mM EDTA. The flow-through was lyophilized, dry protein was dissolved in distilled H_2O, and this solution was passed over a Superdex 30 HiLoad 26/60 size-exclusion column equilibrated with pH 7.0 buffer containing 50 mM sodium phosphate, 50 mM NaCl, and 1 mM DTT. Column fractions eluting at ~150 mL were collected and buffer-exchanged using a series of three HiPrep 26/10 desalting columns equilibrated with pH 8.0 buffer containing 25 mM ammonium bicarbonate. The flow-through was collected and lyophilized to yield dry protein that was used in subsequent NMR studies.

hMms2

Human Mms2 was cloned as a GST fusion protein as previously described (McKenna et al., 2001). [$U-^{15}N$; $U-^{13}C$]–Mms2 protein was expressed in *E. coli* strain BL21(DE3)–RIL as follows: 50 mL of LB containing 50 μg/mL ampicillin and 25 μg/mL chloramphenicol was inoculated with a single colony and grown at 37 °C with aeration to $A_{600} \sim 0.8$. About 2 L of M9 media was prepared in an identical fashion as that for production of [$U-^{15}N$; $U-^{13}C$]–Ub. The M9 media was inoculated with 2 mL of LB culture and grown overnight (~16 hours) at 25 °C with aeration to $A_{600} \sim 0.8$, induced with 0.4 mM IPTG, and incubated for an additional 9 hours.

Cells were harvested by centrifugation, the cell pellets were resuspended in ~70 mL lysis buffer (as prepared for Ub). Cells were lysed by two passes through a French press and the lysate was clarified by centrifugation. The supernatant was then filtered through a Millipore steriflip 0.45 μm vacuum filtration device. The filtered lysate was loaded onto a GSTprep FF 16/10 column equilibrated in pH 7.4 buffer containing 140 mM NaCl, 2.7 mM KCl, 10 mM Na_2HPO_4 and 1.8 mM KH_2PO_4. GST-fusion protein was eluted from the column with buffer containing 50 mM TrisHCl, 10 mM reduced glutathione, pH 8.0. Fractions eluting with glutathione buffer were collected, pooled, and buffer exchanged by passage through three HiPrep 26/10 desalting columns equilibrated with pH 7.0 buffer containing 50 mM TRIS, 150 mM NaCl, 1 mM EDTA, and 1 mM DTT. The flow-through was collected and concentrated to ~5 mL. About 10 μL (20 units) of PreScission protease was added to the concentrated protein and the cleavage reaction was allowed to proceed for 24 hours at 4 °C. The cleaved protein was then purified with a GSTprep FF 16/10 column as described above for the intact fusion protein. The flow-through was collected and further purified by loading 9 mL of protein solution twice onto a HiLoad 26/10 Superdex 75 column equilibrated with buffer containing 50 mM sodium phosphate, 50 mM NaCl, and 1 mM DTT, pH 7.0. The peak fractions eluting at 185–210 mL were pooled and concentrated for NMR studies. In order to stereospecifically assign the methyl groups of hMms2, [$U-^{15}N$; U-10% ^{13}C]–Mms2 was expressed in *E. coli* strain BL21(DE3)-RIPL using the protocol described by Neri et al. (1989).

Expression of unlabeled hMms2 was accomplished in a similar fashion as Ub-K48R. Purification of unlabeled hMms2 was identical to [$U-^{15}N$; $U-^{13}C$]–Mms2.

NMR Spectroscopy

All NMR spectra were obtained using either Varian Unity INOVA 500, 600, or 800 MHz NMR spectrometers. For [$U-^{15}$N; $U-^{13}$C]-hMms2 and [$U-^{15}$N; U-10% ^{13}C]-hMms2, NMR samples were 600 μL for standard 5 mm i.d. NMR tubes, and 300 μL for SHIGEMI microcell NMR tubes, and contained 9:1 H_2O/D_2O with 50 mM phosphate (pH 7.5) 150 mM NaCl, 1 mM DTT, 1 mM DSS, 3 μL of 100× stock protease inhibitor cocktail I (Calbiochem catalog #539131), with ~0.5 mM hMms2 and ~2.0 mM Ub. For [$U-^{15}$N; $U-^{13}$C]-Ub, samples were 300 μL in SHIGEMI microcell NMR tubes with sample conditions same as above, with the exception that the protein concentrations used were ~2.0 mM Ub and ~0.5 mM hMms2. For [$U-^{15}$N]-Ub, the sample used for titration was 600 μL for standard 5 mm i.d. NMR tube with sample conditions same as above, with the exception that the protein concentrations used were ~0.25 mM Ub, and 0, ~0.25, ~0.5, ~0.75, and ~1 mM hMms2.

Chemical shift assignment of Ub

Unambiguous assignment of the Ub main chain atoms was completed at 30 °C using a combination of the HNCACB (Wittekind and Mueller, 1993; Muhandiram and Kay, 1994) and (H)CCTOCSYNNH experiments (Logan et al., 1993; Gardner et al., 1996). Non-aromatic side chain atoms were assigned using the HCCTOCSYNNH and (H)CCTOCSYNNH experiments (Lyons and Montelione, 1993; Logan et al., 1993; Gardner et al., 1996), and the HCCH-TOCSY experiment (Bax et al., 1990, Kay et al., 1993). Aromatic side chains were assigned using a constant-time (Vuister and Bax, 1992) ^{13}C-edited NOESY-HSQC experiment. All spectra were processed using the program NMRPipe (Delaglio et al., 1995), and chemical shift assignment was accomplished using the program Sparky (Goddard and Kneller).

Titration of [^{15}N]-Ub with hMms2

Four 38 μL aliquots of ~3.6 mM hMms2 were titrated into ~0.25 mM [$U-^{15}$N]–Ub at 30 °C, and a 2D ^{1}H–^{15}N–HSQC NMR spectrum was acquired at each titration point. Average chemical shift perturbations for each resonance were calculated using a previously described method (Garrett et al., 1997). Average chemical shift changes that were greater than one standard deviation from the mean were considered significant.

Chemical shift assignment of hMms2 bound to Ub

NMR experiments for chemical shift assignment of hMms2 bound to Ub were collected using a 1:4 [$U-^{13}$C; $U-^{15}$N]-hMms2:unlabelled Ub sample ([hMms2] ~0.5 mM). The main chain atoms of hMms2 were unambiguously assigned using a combination of the HNCA (Kay et al., 1990; Cavanagh et al., 1991; Kay et al., 1992; Muhandiram and Kay, 1994) and HN(CO)CA (Kay et al., 1990; Yamazaki et al., 1994) experiments at 30 °C. Methyl group ^{1}H and ^{13}C assignments were accomplished using the MQ-(H)CC_mH$_m$-TOCSY experiment at 30 °C (Yang et al., 2004). Partial assignments for non-methyl and non-aromatic side chain atoms were obtained in the same fashion as the side chain atoms for Ub, with the exception that the spectra were obtained at 40 °C. The prochiral Val and Leu methyl groups of hMms2 were stereospecifically assigned using a non-constant time ^{1}H–^{13}C–HSQC spectrum obtained from a 1:4 [$U-^{15}$N; U-10% ^{13}C]-hMms2:unlabelled Ub sample at 30°C (Neri et al., 1989).

Ub–hMms2 Intermolecular NOEs

^{1}H–^{1}H NOEs between Ub and hMms2 were identified by analyzing ^{13}C, ^{15}N F_1-filtered, F_3-edited NOESY experiments (Zwahlen et al., 1997) collected for two NMR samples at 30 °C, one containing 1:4 [$U-^{13}$C; $U-^{15}$N]-hMms2:unlabelled Ub and the other containing 1:4 [$U-^{13}$C; $U-^{15}$N]-Ub:unlabelled hMms2. Intermolecular NOE restraints were set to lower and upper bounds of 1.8 and 5.0 Å, respectively.

Structure determination

Protein docking for the hMms2-Ub complex was performed with the HADDOCK (High Ambiguity Driven protein–protein Docking) protocol (Dominguez et al., 2003), using the crystal structures of hMms2 (1j74) and Ub (1ubq) as starting structures, and with intermolecular NOEs as

restraints. The starting structures were fixed as rigid bodies, except for residues in and around the binding face, for which full flexibility was allowed. Out of 200 rigid body docking trials, the top 50 lowest energy structures underwent structural refinement. The ten lowest energy structures from the protocol were subjected to a final refinement in explicit solvent. The energy difference between the highest energy selected structure and the lowest energy omitted structure is 1.67 kcal/mol (the difference between the lowest and highest energy selected structures is 5.72 kcal/mol). The quality of the structural ensemble was assessed using the program Procheck (Laskowski et al., 1993). Changes in accessible surface area for hMms2 and Ub upon binding were calculated using the program STC (Lavigne et al., 2000).

Molecular graphics

Protein structure graphics (Figures 3–7) were produced using the program Pymol (DeLano, 2002).

RCSB PDB accession code

The hMms2–Ub structure has been deposited in the Protein Data Bank under the accession code 1ZGU.

Results

Titration of [U–^{15}N]-Ub with hMms2

Backbone amide $^{1}H_N$ and ^{15}N chemical shift changes for [U–^{15}N]- hMms2 upon titration with Ub have been reported previously (McKenna et al., 2003b). In this study, $^{1}H_N$ and ^{15}N chemical shift changes for [U–^{15}N]-Ub upon titration with hMms2 were determined (Figure 1). Only thirteen of 71 observable backbone amide $^{1}H_N$—^{15}N chemical shifts exhibit a significant change. On this basis, we assume that structural changes for Ub upon binding hMms2 are small. This assumption was also made with respect to the structure of hMms2 upon Ub binding on the basis of our previous work (McKenna et al., 2003a).

Ub–hMms2 Intermolecular NOEs

Intermolecular contacts between hMms2 and Ub were identified using ^{13}C,^{15}N F_1-filtered, F_3-edited NOESY experiments for each of hMms2 and Ub (Figure 2). The interface was initially characterized by assigning methyl–methyl NOEs between the two proteins. Non-methyl and non-aromatic side chain protons for hMms2 were assigned with the aid of spectra collected at 40 °C and were subsequently assigned in the intermolecular NOE spectra. A total of 51 intermolecular NOEs were assigned, and of these, 27 were methyl–methyl NOEs.

Description of the structure

The structures of hMms2 and Ub in the complex are very similar to the free structures of the individual proteins, superimposing with backbone rmsds of 0.81 ± 0.13 Å and 0.77 ± 0.21 Å for hMms2 and Ub, respectively. This is due in large part to the fact that only regions that were involved in intermolecular NOEs, and adjacent regions, were unconstrained. In the family of ten structures, there are no NOE violations greater than 0.1 Å, the backbone rmsd value is 0.97 ± 0.14 Å to the average structure, the side chain heavy atom rmsd is 1.18 ± 0.12 Å (Figure 3), and 89.6/9.8% of residues are in the most favored/additionally allowed regions of the Ramachandran plot. In the family of ten structures generated using the HADDOCK protocol, hMms2 and Ub bury 296 ± 42 and 288 ± 23 Å^2 of polar accessible surface area respectively, as well as 412 ± 33 and 406 ± 43 Å^2 of nonpolar surface area, respectively.

Discussion

Description of the interface between Ub and hMms2

The structure of the hMms2–Ub complex presented here indicates that strands 1–3 from the single β-sheet face of hMms2, are involved in binding to strands 1, and 3–5 of the single β-sheet face of Ub. The binding interface of Ub is comprised in part by the hydrophobic residues Leu8, Ile44, and Val70 (Figure 4). Indeed, several intermolecular NOEs are observed between the methyl protons of these residues, and protons of hMms2 (Figure 2). These Ub residues are also involved in interactions between Ub and the Ub-binding proteins CUE (Kang et al., 2003; Prag et al., 2003) and UIM (Swanson et al., 2003). At the periphery

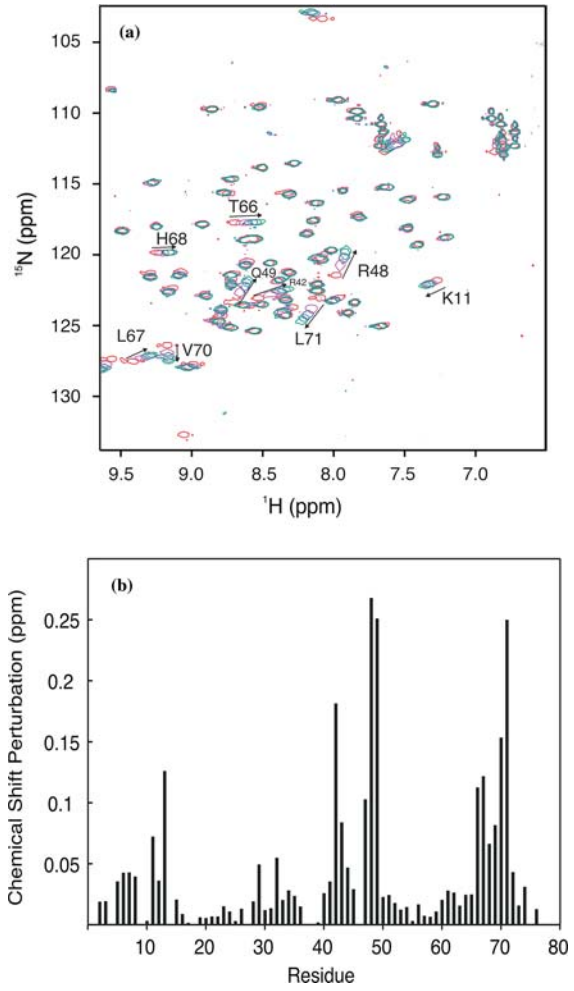

Figure 1. [^{15}N]-Ub backbone amide chemical shift changes during titration of hMms2. (a) Superposition of Ub ^{1}H–^{15}N HSQC spectra collected for various approximate values of [hMms2]/[Ub] ratios: 0:1, 1:1, 2:1, 3:1 and 4:1. Only those cross-peaks that were affected by complex formation are labelled. (b) Plot of weighted average chemical shift perturbations by residue number, as given by $\delta_{av} = [(\Delta\delta_{NH}^2 + \Delta\delta_N^2/25)/2]^{1/2}$ (Garrett et al., 1997).

of the interface there is a potential salt bridge between Glu41 Oγ of hMms2 and Arg48 Hη of Ub, which is ~5 Å away. The side chain of Ub-Ile44 is involved in close contacts with a hydrophobic "patch" formed by hMms2 residues Met54, Ile56, and Ile67, and is almost completely buried by these residues (Figure 4). Additional NOE contacts are observed between Val70 and Leu8 of Ub and Ile56 of hMms2. The side chain of Ile67 of hMms2 forms close contacts with Ub residues Ile44, Arg42, and Gln49. At the periphery of the binding interface, Thr52 of hMms2 and Arg48 of Ub are in close contact. Further contacts at the periphery of the binding interface include Thr35 of hMms2 and Leu8 and Val70 of Ub, and Ala46 of Ub to Gly39 and Gln28 of hMms2.

The total buried surface area in the hMms2–Ub interaction is 1402 ± 72 Å^2. This value is higher than for other reported ubiquitin binding domain interactions (1120 ± 66 Å^2 for CUE [1otr] and 1054 ± 66 Å^2 UIM [1q0w], using the first ten structures from each ensemble), with a corresponding smaller K_D (98 ± 15 μM compared to 155 ± 9 μM for the CUE-Ub and 277 ± 8 μM for the UIM-Ub interactions (Kang et al., 2003; Swanson et al., 2003)).

Implications for catalysis of Lys63-linked polyubiquitin chains

Lys63-linked polyubiquitin chains play important functional roles within eukaryotic cells, and the Mms2–Ubc13 complex is the enzyme responsible for catalysis of these chains. A superposition of the structure of hMms2 within the hMms2–Ub complex presented herein and the structure of hMms2 within the hMms2–hUbc13 heterodimer determined previously (1j7d), positions Lys63 of Ub proximal to the binding interface between hMms2 and hUbc13 (Figure 5). In this orientation, the ε-amino group of Lys63 is 12 ± 1 Å away from the active site cysteine of hUbc13. In order to better assess the biological impact of the hMms2–Ub structure presented herein, we have docked Ub to the hMms2–hUbc13 protein complex employing the HADDOCK protocol as described for the Ub–hMms2 complex, and using only Ub–hMms2 intermolecular NOEs measured in the absence of hUbc13 (see Methods). Using this approach, all of the intermolecular distance restraints are satisfied when hUbc13 is included in the docking protocol. For example, the intermolecular NOE energy when hUbc13 is present in the docking protocol is $(14 \pm 8) \times 10^{-3}$ kcal mol^{-1} compared to $(9.0 \pm 0.6) \times 10^{-3}$ kcal mol^{-1} in the absence of hUbc13. In addition, there are no NOE violations greater than 0.1 Å in the presence or absence of hUbc13. In the family of ten structures calculated in the presence of hUbc13, the ε-amino group of Ub-Lys63 is 9 ± 2 Å from the active site cysteine of hUbc13 (Figure 6a). In this orientation, the ε-amino group of Ub-Lys63 is predominantly

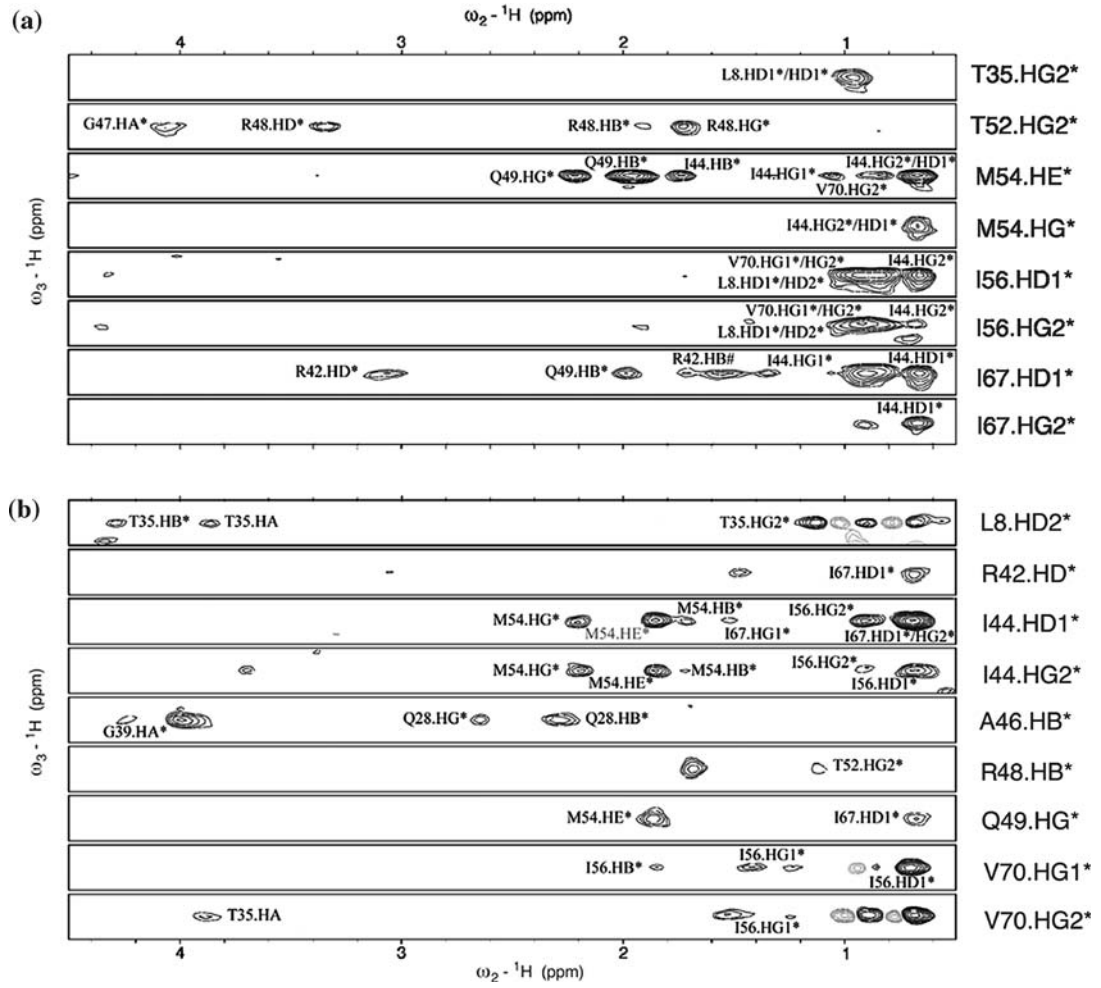

Figure 2. Strips taken from the ^{13}C, ^{15}N F_1-filtered, F_3 -edited NOESY experiments. Intermolecular NOEs, or close contacts ranging from 1.8–5.0 Å between $^{13}C/^{15}N$-hMms2 and Ub are shown in (a), and NOE contacts between $^{13}C/^{15}N$-Ub and hMms2 are shown in (b). Unlabelled peaks were unassigned due to either ambiguity or lack of chemical shift data.

involved in hydrogen bonds with the either the backbone carbonyl of Pro120 or Leu121 of hUbc13, and is positioned at the mouth of a cleft that leads directly to the active site of hUbc13 (Figure 6b). The ensemble of structures shown in Figure 6a is consistent with the following experimental observations. The backbone amide ^1H_N—^{15}N chemical shift changes for hMms2 induced by Ub binding in the presence and absence of hUbc13 suggest that the surface of hMms2 involved in Ub binding is similar (McKenna et al., 2003b). Furthermore, comparison of the ensemble of Ub–hMms2–hUbc13 structures shown in Figure 6a to the ensemble of Ub–hMms2 structures shown in Figure 3 indicates that the increase in buried surface area when hUbc13 is present is not large (hMms2 buries 1402 ± 72 Å^2 and hMms2–hUbc13 buries 1738 ± 86 Å^2, upon interaction with Ub). These small changes in buried surface area are consistent with the observation that we have not detected chemical shift changes in ^1H_N–^{15}N HSQC spectra of ^{15}N-hUbc13 upon addition of acceptor Ub in the presence and absence of hMms2 (McKenna et al., 2003b). Finally, the affinity of acceptor Ub is not radically greater ($K_D = 28 \pm 6$ μM) than that for hMms2 alone ($K_D = 98 \pm 15$ μM) (3 ± 1 fold greater) (McKenna et al., 2003a).

Interestingly, hUbc13-Asp81 has been shown to be critical for the synthesis of Lys63-linked di-Ub chains (VanDemark et al., 2001). For

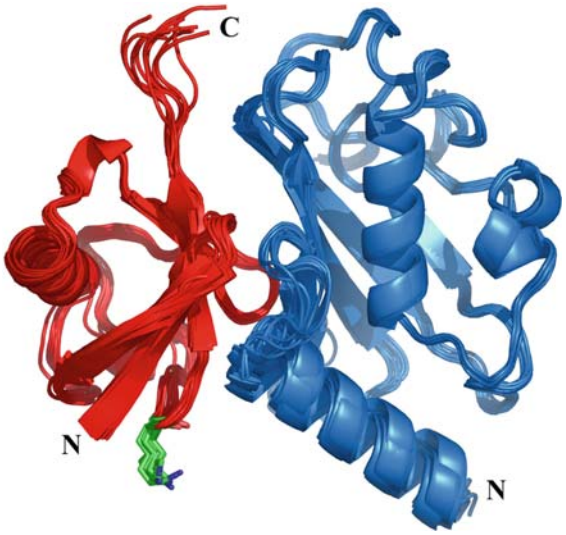

Figure 3. Ensemble of ten structures for the hMms2–Ub complex generated using the HADDOCK protocol. The backbone atoms of hMms2 are shown as a blue cartoon, and the backbone atoms of Ub are shown as a red cartoon. Lys63 of Ub is shown in green in the stick representation.

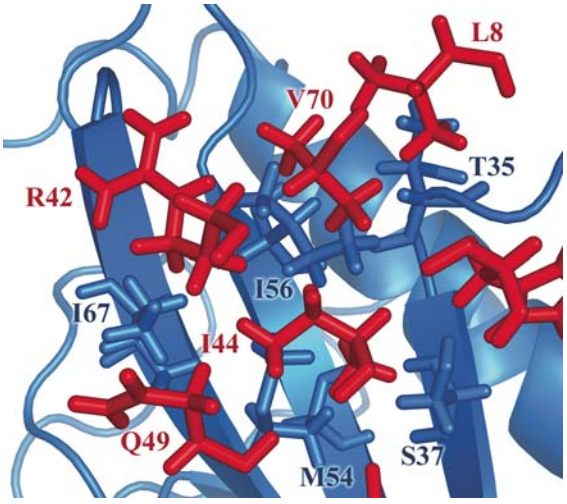

Figure 4. Intermolecular interactions at the hMms2–Ub binding interface. The backbone atoms of hMms2 are shown in the cartoon representation (blue), with side chains that interact with Ub shown in the stick representation. Ub residues for which intermolecular NOEs to hMms2 are observed are shown in the stick representation (red).

example, mutation of Asp81 to Ala results in impairment of catalysis, whereas mutation to Arg abolishes di-Ub formation. On the basis of these mutational studies, it has been suggested that the catalytic role of hUbc13-Asp81 is to

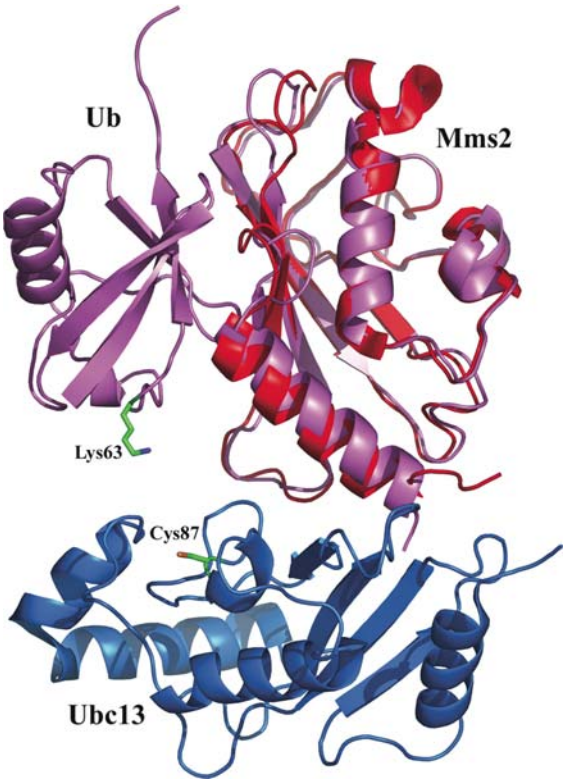

Figure 5. Superposition of hMms2-Ub on the crystallographically determined hMms2–hUbc13 structure. The backbone atoms of the average hMms2–Ub structure determined in the present study (violet cartoon), are superimposed on the backbone atoms of the hMms2–hUbc13 structure (1j7d), (red-blue cartoon). Lys63 of Ub and the active site cysteine of hUbc13 are shown in green in the stick representation.

position Ub-Lys63 within the active site (VanDemark et al., 2001). If we assume that the role of hUbc13-D81 is to position Lys63, and impose a distance restraint of 2.5 ± 0.5 Å between the ε-amino nitrogen of Ub-Lys63 and either of the side chain carboxyl oxygen atoms of hUbc13-D81 during docking of Ub with the hMms–hUbc13 heterodimer using the HADDOCK protocol (as implemented for the hMms2–Ub structure), then all of the NOE distance restraints between hMms2 and Ub measured in the absence of hUbc13 are satisfied (intermolecular NOE energy of $(17 \pm 10) \times 10^{-3}$ kcal mol^{-1}), with no violations greater than 0.3 Å, and only one violation greater than 0.1 Å in the family of ten structures.

In light of this analysis, it is of interest to compare this model for the interaction of Ub-Lys63 with the active site of hUbc13 with the

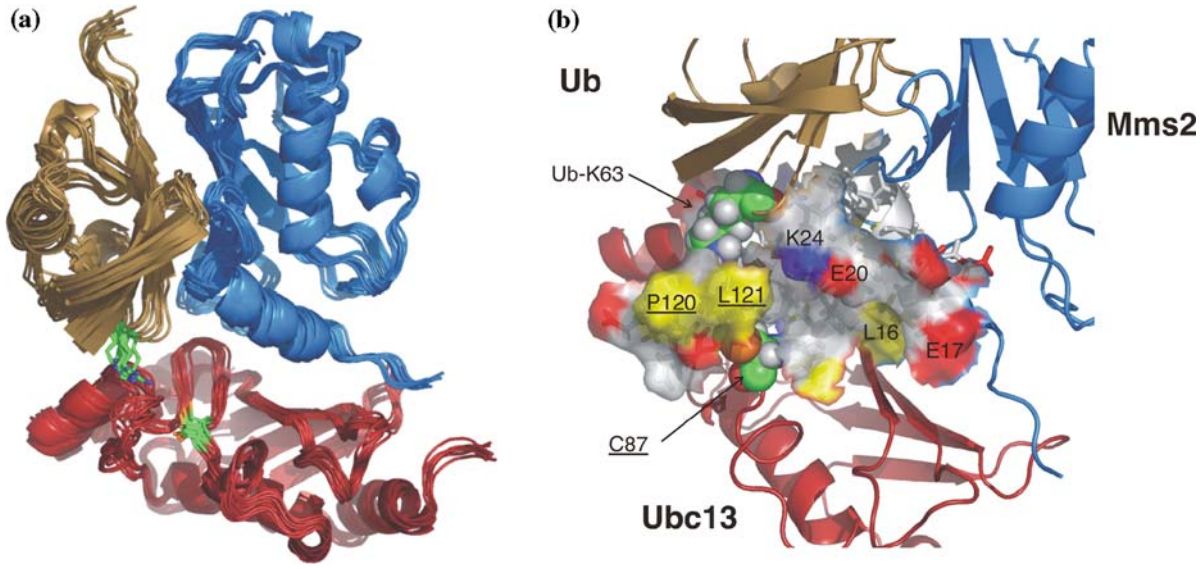

Figure 6. Model for the acceptor Ub-hMms2-hUbc13 ternary complex generated using the HADDOCK protocol. (a) Ensemble of ten structures calculated in the same fashion as the ensemble of Ub–hMms2 structures shown in Figure 3 with the exception that the coordinates of hUbc13 were included. The backbone atoms of hUbc13, hMms2, and Ub are shown as red, blue, and gold cartoons, respectively. (b) Surface representation of the active site cleft for the hMms2–hUbc13 heterodimer. Polar atoms of the surface of the active site are colored in white, negatively charged atoms are colored red, positively charged atoms are colored blue, and hydrophobic atoms are colored yellow. Labels for residues from hUbc13 are indicated in underline. The atoms of Ub-Lys63 and hUbc13–Cys87 are shown as spheres.

crystallographically determined structure of the E2 Ubc9 in complex with its substrate RanGAP1 (Bernier-Villamor et al., 2002). Ubc9 is a SUMO E2 enzyme that attaches the ubiquitin-like modifier SUMO to Lys526 of RanGAP1, and this process is important in nucleocytoplasmic transport. Figure 7a shows the superposition of Ubc9 (in complex with RanGAP1, 1kps) superimposed on hUbc13 (in complex with hMms2, 1j7d). There are key amino acid differences in the active site of hUbc13 compared to Ubc9. Leu121 in hUbc13 is equivalent to Ala129 in Ubc9, but the side chains of these residues occur in very different positions in comparison to other active site residues such as Cys87 (hUbc13) and Cys93 (Ubc9), Asn79 (hUbc13) and Asn85 (Ubc9). In addition, the bulky aromatic side chain of Tyr87 in Ubc9 replaces Asp81 of hUbc13, a residue important for catalysis (VanDemark et al., 2001). Figure 7b shows the superposition between Ubc9 and hUbc13 within the acceptor Ub–hMms2–hUbc13 structure closest to the average structure, determined using HADDOCK docking as described above with the assumption that hUbc13-Asp81 is responsible for positioning Ub-Lys63. As shown in Figure 7b, if approach of substrate Ub-Lys63 to the active site cysteine of hUbc13 is similar to that for Ubc9, it would be involved in a steric clash with Leu121. For Ubc9 on the other hand, given the active site orientation shown in 7a, the substrate lysine cannot approach the active site cysteine from directly above due to steric clashes with Ubc9-Tyr87 and Ubc9-Ala129. The structural differences between the active sites of Ubc9 and hUbc13 may be important in the specific recognition and correct positioning of substrate lysine residues destined for SUMO conjugation rather than ubiquitination.

Recently, it has been demonstrated that mutation of either of the side chains Ub-Ile44 and yeast Mms2-Ile57 (equivalent to hMms2-Ile67) to alanine results in a 10- to 20-fold inhibition of Lys63-linked polyubiquitin chain synthesis, suggesting that the acceptor Ub binding site on Mms2 is necessary for *in vivo* chain assembly (Tsui et al., 2005). In the present work, we have demonstrated a direct interaction between Ub-Ile44 and hMms2-Ile67. In addition, the position of Ub-Lys63 within the hMms2–Ub structure is consistent with proposed mechanisms of Lys63-linked chain catalysis.

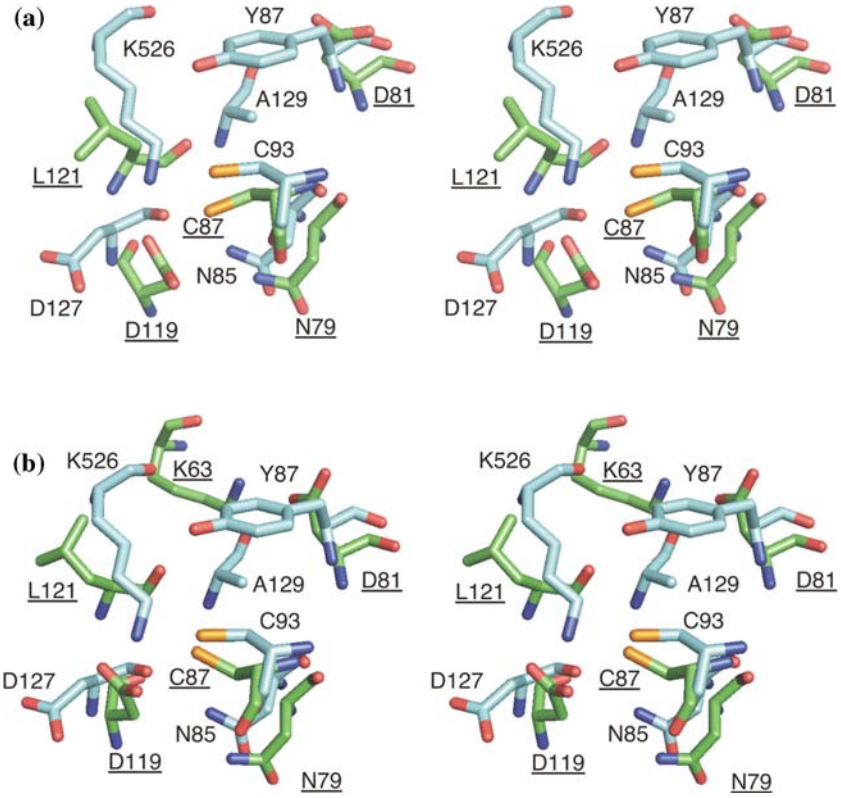

Figure 7. Comparison of the structures of Ubc9 and hUbc13. (a) Divergent stereo view of the structure of Ubc9 (in complex with RanGAP1, 1kps) superimposed on the structure of hUbc13 (in complex with hMms2, 1j7d). (b) Divergent stereo view of the structure of Ubc9 (in complex with RanGAP1, 1kps) superimposed on the model of the ternary complex of acceptor Ub–hMms2–hUbc13 determined herein using intermolecular NOEs between hMms2 and Ub and assuming that hUbc13–Asp81 is involved in hydrogen bonding interactions with Ub–Lys63. The side chain carbon atoms of Ubc9/RanGAP1 are shown in light blue and those for hUbc13/Ub are shown in green. Labels indicating hUbc13 residues are shown in underline.

Thus, the structural basis for the functional data reported by Pickart and coworkers (Tsui et al., 2005) is a direct disruption of the Ub-Ile-44 hMms2-Ile67 interaction, leading to impaired Lys63 chain catalysis.

Finally, the close proximity of Ub Arg48 to the binding interface in the hMms2–Ub complex suggests that Lys48 of the wild type Ub could potentially be excluded as a site for canonical Lys48-linked chain formation. However, in the present structure, as in the Tsg101–Ub structure (Sundquist et al., 2004) (*vide supra*), Arg/Lys48 is involved in contacts at the periphery of the interface, and remains partly solvent exposed.

Comparison to other Ub-binding protein complexes

Recently, the structure of the UEV domain of Tsg101 (Vps23p in yeast), has been solved in complex with Ub by X-ray crystallography (Sundquist et al., 2004). Interestingly, the structural basis of the Tsg101–Ub interaction is distinct from that of hMms2–Ub. Whilst both UEV domains bind to a similar hydrophobic surface on Ub, Tsg101 does not bind *via* the single β-sheet face as observed for the hMms2–Ub interaction. Tsg101 binds Ub through the loop of an extended β-tongue motif, which consists of strands 1 and 2 of the UEV domain. This difference is not entirely surprising, given Tsg101 and Mms2 play very different functional roles in eukaryotic cells. Furthermore, from an evolutionary standpoint, the UEV domain of Tsg101 is further diverged from the canonical E2 fold than Mms2 (Pornillos et al., 2002).

Uev1a, a UEV involved in NF-κB activation (Deng et al., 2000; Wang et al., 2001), is a close relative of hMms2 (Xiao et al., 1998). Both Uev1a and hMms2 form a stable heterodimer with

hUbc13 in order to catalyze the formation of Lys63-linked polyubiquitin chains (Deng et al., 2000). hUev1a shares 92% core sequence identity with hMms2 (Xiao et al., 1998), and adopts a nearly identical fold (data unpublished). Thus, it is reasonable to expect that the Uev1a–Ub interaction is similar to that for hMms2–Ub, particularly considering the fact that the putative Ub binding site of hUev1a is identical in sequence to hMms2.

Conclusion

In the current study we have used solution state NMR spectroscopy to produce a structure of the hMms2–Ub complex. The binding interface involves many close contacts between the side chains of Met54, Ile56, and Ile67 on hMms2, and Ile44, Val70, and Leu8 on Ub. The structure is consistent with a recent study by Pickart and co-workers (Tsui et al., 2005) that demonstrates the necessity of both Ile67 of hMms2 and Ile44 of Ub in Lys63 chain assembly.

Acknowledgement

We would like to thank the Canadian National High Field NMR Centre (NANUC) for their assistance and use of the facilities. Operation of NANUC is funded by the Canadian Institutes of Health Research (CIHR), the National Science and Engineering Research Council of Canada (NSERC) and the University of Alberta. We thank Deryk Webb for spectrometer maintenance, Yanni Batsiolas for computer support, and Lewis E. Kay for pulse sequences. This research was supported by grants from the CIHR and the Alberta Heritage Foundation for Medical Research (AHFMR).

References

Bax, A., Clore, G.M. and Gronenborn, A.M. (1990) *J. Magn. Reson.*, **88**, 425–431.
Ben-Neriah, Y. (2002) *Nat. Immunol.*, **3**, 20–26.
Bernier-Villamor, V., Sampson, D.A., Matunis, M.J. and Lima, C.D. (2002) *Cell*, **108**, 345–356.
Broomfield, S., Chow, B.L. and Xiao, W. (1998) *Proc. Natl. Acad. Sci. USA*, **95**, 5678–5683.
Cavanagh, J., Palmer, A.G., Wright, P.E. and Rance, M. (1991) *J. Magn. Reson.*, **91**, 429–436.
Chan, N.L. and Hill, C.P. (2001) *Nat. Struct. Biol.*, **8**, 650–652.
Delaglio, F., Grzesiek, S., Vuister, G.W., Zhu, G., Pfeifer, J. and Bax, A. (1995) *J. Biomol. NMR*, **6**, 277–293.
DeLano, W.L. (2002) *DeLano Scientific* San Carlos, CA, USA.
Deng, L., Wang, C., Spencer, E., Yang, L., Braun, A., You, J., Slaughter, C., Pickart, C. and Chen, Z.J. (2000) *Cell*, **103**, 351–361.
Dominguez, C., Boelens, R. and Bonvin, A.M.J.J. (2003) *J. Am. Chem. Soc.*, **125**, 1731–1737.
Gardner, K.H., Konrat, R., Rosen, M.K. and Kay, L.E. (1996) *J. Biomol. NMR*, **8**, 351–356.
Garrett, D.S., Seok, Y.J., Peterkofsky, A., Clore, G.M. and Gronenborn, A.M. (1997) *Biochemistry*, **36**, 4393–4398.
Glickman, M.H. and Ciechanover, A. (2002) *Physiol. Rev.*, **82**, 373–428.
Goddard, T. D. and Kneller, D. G. University of California, San Francisco.
Haglund, K., Di Fiore, P.P. and Dikic, I. (2003) *Trends Biochem. Sci.*, **28**, 598–603.
Hicke, L. (2001) *Nat. Rev. Mol. Cell. Biol.*, **2**, 195–201.
Hicke, L., Schubert, H.L. and Hill, C.P. (2005) *Nat. Rev. Mol. Cell. Biol.*, **6**, 610–621.
Hoege, C., Pfander, B., Moldovan, G.L., Pyrowolakis, G. and Jentsch, S. (2002) *Nature*, **419**, 135–141.
Hofmann, R.M. and Pickart, C.M. (1999) *Cell*, **96**, 645–653.
Kang, R.S., Daniels, C.M., Francis, S.A., Shih, S.C., Salerno, W.J., Hicke, L. and Radhakrishnan, I. (2003) *Cell*, **113**, 621–630.
Kay, L.E., Ikura, M., Tschudin, R. and Bax, A. (1990) *J. Magn. Reson.*, **89**, 496–514.
Kay, L.E., Keifer, P. and Saarinen, T. (1992) *J. Am. Chem. Soc.*, **114**, 10663–10665.
Kay, L.E., Xu, G.Y., Singer, A.U., Muhandiram, D.R. and Forman-Kay, J.D. (1993) *J. Magn. Reson. B*, **101**, 333–337.
Laskowski, R.A., MacArthur, M.W., Moss, D.S. and Thorton, J.M. (1993) *J. Appl. Crystallogr.*, **26**, 283–290.
Lavigne, P., Bagu, J.R., Boyko, R., Willard, L., Holmes, C.F. and Sykes, B.D. (2000) *Protein Sci.*, **9**, 252–264.
Logan, T.M., Olejniczak, E.T., Xu, R.X. and Fesik, S.W. (1993) *J. Biomol. NMR*, **3**, 225–231.
Lyons, B.A. and Montelione, G.T. (1993) *J. Magn. Reson. B*, **101**, 206–209.
McKenna, S., Hu, J., Moraes, T., Xiao, W., Ellison, M.J. and Spyracopoulos, L. (2003a) *Biochemistry*, **42**, 7922–7930.
McKenna, S., Moraes, T., Pastushok, L., Ptak, C., Xiao, W., Spyracopoulos, L. and Ellison, M.J. (2003b) *J. Biol. Chem.*, **278**, 13151–13158.
McKenna, S., Spyracopoulos, L., Moraes, T., Pastushok, L., Ptak, C., Xiao, W. and Ellison, M.J. (2001) *J. Biol. Chem.*, **276**, 40120–40126.
Miura, T., Klaus, W., Gsell, B., Miyamoto, C. and Senn, H. (1999) *J. Mol. Biol.*, **290**, 213–228.
Moraes, T.F., Edwards, R.A., McKenna, S., Pastushok, L., Xiao, W., Glover, J.N. and Ellison, M.J. (2001) *Nat. Struct. Biol.*, **8**, 669–673.
Muhandiram, D.R. and Kay, L.E. (1994) *J. Magn. Reson. Ser. B*, **103**, 203–216.
Neri, D., Szyperski, T., Otting, G., Senn, H. and Wuthrich, K. (1989) *Biochemistry*, **28**, 7510–7516.
Pornillos, O., Alam, S.L., Rich, R.L., Myszka, D.G., Davis, D.R. and Sundquist, W.I. (2002) *Embo. J.*, **21**, 2397–2406.
Prag, G., Misra, S., Jones, E.A., Ghirlando, R., Davies, B.A., Horazdovsky, B.F. and Hurley, J.H. (2003) *Cell*, **113**, 609–620.
Sambrook, S., Fritch, E.F. and Maniatis, T. (1989) *Molecular Cloning: A Laboratory Manual* Cold Spring Harbor Laboratory Press, New York, NY.

Schnell, J.D. and Hicke, L. (2003) *J. Biol. Chem*., **278**, 35857–35860.
Slupsky, C.M., Kay, C.M., Reinach, F.C., Smillie, L.B. and Sykes, B.D. (1995) *Biochemistry*, **34**, 7365–7375.
Sundquist, W.I., Schubert, H.L., Kelly, B.N., Hill, G.C., Holton, J.M. and Hill, C.P. (2004) *Mol. Cell*, **13**, 783–789.
Swanson, K.A., Kang, R.S., Stamenova, S.D., Hicke, L. and Radhakrishnan, I. (2003) *Embo. J*., **22**, 4597–4606.
Tsui, C., Raguraj, A. and Pickart, C.M. (2005) *J. Biol. Chem*., **280**, 19829–19835.
VanDemark, A.P., Hofmann, R.M., Tsui, C., Pickart, C.M. and Wolberger, C. (2001) *Cell*, **105**, 711–720.
Vuister, G.W. and Bax, A. (1992) *J. Magn. Reson*., **98**, 428–435.
Wang, C., Deng, L., Hong, M., Akkaraju, G.R., Inoue, J. and Chen, Z.J. (2001) *Nature*, **412**, 346–351.
Wittekind, M. and Mueller, L. (1993) *J. Magn. Reson. B*, **101**, 201–205.
Xiao, W., Lin, S.L., Broomfield, S., Chow, B.L. and Wei, Y.F. (1998) *Nucleic Acid Res*., **26**, 3908–3914.
Yamazaki, T., Lee, W., Arrowsmith, C.H., Muhandiram, D.R. and Kay, L.E. (1994) *J. Am. Chem. Soc*., **116**, 11655–11666.
Yang, D.W., Zheng, Y., Liu, D.J. and Wyss, D.F. (2004) *J. Am. Chem. Soc*., **126**, 3710–3711.
Zwahlen, C., Legault, P., Vincent, S.J.F., Greenblatt, J., Konrat, R. and Kay, L.E. (1997) *J. Am. Chem. Soc*., **119**, 6711–6721.